Surface Rheology and Phase Transitions of Monolayers of Phospholipid/Cholesterol Mixtures

Marcel Vrânceanu,*† Karin Winkler,* Hermann Nirschl,† and Gero Leneweit*
*Carl Gustav Carus-Institute, 75223 Niefern-Öschelbronn, Germany; and †University of Karlsruhe (Technische Hochschule), Institute of Mechanical Process Engineering and Mechanics, 76131 Karlsruhe, Germany

ABSTRACT The dynamic surface elasticity and the surface dilational viscosity of three binary phospholipid/cholesterol mixtures were determined with axisymmetric drop shape analysis on a harmonically oscillating pendent drop. Dipalmitoylphosphatidylcholine, dimyristoylphosphatidylcholine, and dioleoylphosphatidylcholine were used to explore the rheological properties and phase transitions of mixtures of saturated and unsaturated phospholipids with cholesterol. The growth rates for surface dilational viscosity and dynamic elasticity are parallel for all film pressures studied. Characteristic breaks and plateaus could be found for these growth rates, indicating phase transitions. For dipalmitoylphosphatidylcholine/cholesterol and dimyristoylphosphatidylcholine/cholesterol mixtures, phase diagrams with six regions separated by phase boundaries were found, which are in good agreement with phase transitions reported in the literature for static measurements of isotherms and isobars on a Langmuir film balance and from fluorescence microscopy. Some phase boundaries were only found by dynamic, but not by static, elasticity measurements. Imaging methods revealed phase separations produced by the formation of condensed stoichiometric complexes leading to micron-sized and mostly circular domains. The effects of these complexes on monolayer rheology in liquid/liquid phases is described. Furthermore, liquid/solid and solid phase transitions are discussed.

INTRODUCTION

Rheological properties, the separation of immiscible phases, and phase transitions of phospholipids and their mixtures with cholesterol are all of fundamental importance for the understanding of physiological processes at cell membranes such as membrane fusion, adhesion, endocytosis, signal transduction, or lipid sorting and protein trafficking ((1) and its references). The use of phospholipid/cholesterol mixtures in the preparation of liposomes for different applications in medicine has further kindled interest in this topic. It has been shown previously that both bilayers and monolayers exhibit separation of immiscible phases for various lipid mixtures that can be visualized as isolated micron-sized domains. Because monolayers are more easily accessible by fluorescence microscopy and other methods that visualize phase transitions, as well as by rheological methods, many studies focus on monolayers at gas/water interfaces. Their correlations and discrepancies to phase separations in bilayers have been discussed by several authors (2,3).

There are fundamental differences in the rheology and phase formation of phospholipids consisting of either saturated or unsaturated fatty acids. These differences prevail in binary mixtures with cholesterol. To better characterize them, three ubiquitous phospholipids with a phosphatidylcholine headgroup and either saturated fatty acids (dipalmitoylphosphatidylcholine (DPPC) and dimyristoylphosphatidylcholine (DMPC)) or monounsaturated fatty acids (dioleoylphosphatidylcholine (DOPC)) were chosen for this study.

Various methods have been used to characterize rheology, phase separations, and transitions of the pure phospholipids and their mixtures with cholesterol. Classically, film pressure versus area isotherms are produced on a Langmuir film balance. Static dilational elasticity is the derivative of the isotherm in thermodynamic equilibrium (Eq. 1). Isotherms are reported for DPPC (4–9), DMPC (10–12), DOPC (4), binary DPPC/cholesterol (9,13), binary DMPC/cholesterol (14–17), and ternary DOPC/DPPC/cholesterol mixtures (3). To obtain dynamic results of surface elasticity and dilational viscosity, monolayers on a Langmuir film balance were studied with an oscillating barrier at a broad range of frequencies, as described previously for DPPC (18–22) and DOPC (23). Surface shear viscosity of DPPC was studied with a shear rheometer (21,22,24).

Area oscillations of drop or bubble surfaces can be performed with profile analysis tensiometry using the principle of axisymmetric drop shape analysis. Here, monolayer compression and expansion forces are more homogeneously applied over the whole area than with a Langmuir film balance. Axisymmetric drop shape analysis was used to study DPPC (8,25–27) and other phospholipid monolayers at the air/water interface (8,25–29), chloroform/water interface (25,26,30), *n*-dodecane/water interface (26,31), or dichloromethane/water interface (32). Alternatively, to a pendent drop, profile analysis tensiometry can also be used to study a captive bubble under prescribed oscillations. This was performed for DPPC (4,33), DMPC (34), and DOPC (4).

In addition to rheological measurements, different imaging methods have been used to characterize phase separations and transitions of DPPC, DMPC, DOPC, and their mixtures with cholesterol as monolayers on Langmuir troughs. Using a

Submitted January 19, 2007, and accepted for publication October 31, 2007.

Address reprint requests to Gero Leneweit, E-mail: gero.leneweit@carus-institut.de.

Editor: Petra Schwille.

0006-3495/08/05/3924/11 $2.00

doi: 10.1529/biophysj.107.104851

fluorescently labeled phospholipid, the coexistence of separated immiscible phases and their transitions can be proved with fluorescence microscopy, which was performed for DPPC (4,13,35–39), DOPC (4,36), DPPC/cholesterol (37–39), DMPC/cholesterol (15,39–42), DOPC/cholesterol (40,41), and DPPC/DOPC/cholesterol (2,3). Other imaging methods include Brewster angle microscopy (12,18,30), ellipsometry (19,35), and near-field scanning optical microscopy (43,44), all of which have been used to study DPPC and DMPC. DPPC and DMPC also have been investigated using atomic force microscopy in binary mixtures with cholesterol (11,44) as Langmuir-Blodgett films on solid substrates. Further, fluorescence microscopy was used to visualize separation of immiscible phases on giant bilayer vesicles (2,45,46).

The formation of condensed complexes in a stoichiometric ratio of phospholipids/cholesterol was reviewed by McConnell and Radhakrishnan (47). This formation has been shown to cause the separation of two immiscible liquid phases, which leads to the appearance of (approximately) circular domains. Their size range spans from the nanometer scale to 30 μm. Domains in the micrometer range can be visualized. These domains can either consist of condensed complexes or of a second phase, depending on the phase fraction. When the phospholipid/cholesterol mixture corresponds to the stoichiometric ratio, miscibility is given at all film pressures. For mixing ratios with a lower cholesterol content than the stoichiometric ratio, the condensed complexes separate from a phase that is rich in phospholipids. In the phase diagram, this region of immiscibility is the so called α-region. In the opposite case of mixing ratios, where the cholesterol content is higher than the stoichiometric ratio, the condensed complexes separate from a phase that is rich in cholesterol. In the phase diagram, the corresponding region of immiscibility is called the β-region.

Here we present the results of surface dilational viscosity and elasticity measurements for DPPC, DMPC, and DOPC in binary mixtures with cholesterol for the full range of film pressures accessible with a profile analysis tensiometry. We compare the phase transition boundaries of our rheological data with those found on a Langmuir film balance for film pressure/area isotherms and for fluorescence microscopy.

BACKGROUND

Axisymmetric drop shape analysis allows the determination of surface tension σ, film pressure Π, surface dilational viscosity η, and surface elasticity ε for a monolayer present at the liquid/liquid or liquid/gas interface. The main principle is to determine the surface tension of a liquid from the shape of a pendent drop. Surface tension (σ) is calculated by fitting the drop shape to the Young-Laplace equation. Film pressure ($\Pi = \sigma_0 - \sigma_L$) is the difference of the surface tension σ_0 of the pure subphase (water) to that of the lipid monolayer σ_L.

The response of the surface tension to harmonic area oscillations provides information about the rheological properties of monolayers. Surface elasticity (ε) in thermodynamic equilibrium is determined as follows:

$$\varepsilon = \frac{d\sigma}{d\ln A} = \frac{d\sigma}{dA}A, \tag{1}$$

where $d\sigma$ describes the infinitesimal surface tension gradients on a relative variation of the area A. It was shown by Loglio et al. (48) that a complex elasticity modulus E can be determined as follows:

$$E(i\omega) = \frac{F\{\delta\sigma(t)\}}{F\{\delta \ln A(t)\}}, \tag{2}$$

where F denotes the Fourier transformation operator; $\omega = 2\pi f$ is the circular frequency; t is the time; $\delta \ln A(t)$ is the variation of the relative surface area with the frequency f; and $\delta\sigma(t)$ is the surface tension response. Eq. (2) is only applicable when the time dependent area variations are small enough to produce a linear relation between $\delta \ln A(t)$ and $\delta\sigma(t)$. The complex elasticity modulus can be displayed as follows (49):

$$\begin{aligned} E(i\omega) &= E'(\omega) + iE''(\omega) = |E|\exp(i\theta)\ with\ |E| \\ &= \sqrt{E'^2 + E''^2},\ \tan\theta = E''/E', \end{aligned} \tag{3}$$

where θ is the phase angle between the harmonic area oscillation and surface tension response. Dynamic surface elasticity ε and dilational viscosity η can be derived from Eq. (3) as follows:

$$\varepsilon(\omega) = E'(\omega); \quad \eta(\omega) = \frac{E''(\omega)}{\omega} = \frac{\varepsilon\tan\theta}{\omega}.$$

MATERIALS AND METHODS

Materials

DPPC, DMPC, and DOPC were obtained from Lipoid (Ludwigshafen, Germany) with estimated purity of >99%. Cholesterol (standard for chromatography) with purity >99% was obtained from Sigma-Aldrich (Taufkirchen, Germany). Chloroform with purity >99% (Roth, Karlsruhe, Germany) was used as spreading solvent. All materials were used without further purification. Bidistilled water of a purity approved for intravenous use was used as a subphase. All experiments with DPPC and DOPC were performed at ambient temperature, in the range 26.5°C ± 1.6°C; the precise temperature is given in the legend of each figure. Because the main phase transition T_m of DMPC is at T_m = 23.5°C, all measurements with DMPC were conducted in a temperature-controlled chamber at 20.0°C, 25.0°C, and 30.0°C with an accuracy of ±0.1°C. To avoid lipid oxidation, argon was flowing constantly through the measurement chamber. The argon flow was saturated with water vapor by bubbling through water in a bottle. Water evaporation of the drop subphase was compensated by the tensiometer dosing system (PAT-1; Sinterface, Berlin, Germany).

Measurement technique

All details of the measurement procedure, tensiometer calibration, effects of the dynamic parameters (i.e., oscillation amplitude a and frequency f, on ε and η, assessment of higher harmonics in the Fourier transformation and the technique for lipid deposition) are described in a separate publication (27).

Therefore, only a brief summary will be given here. The dynamic surface properties of monolayers were measured with a pendent drop tensiometer (Sinterface) (29).

The pendent drop was formed at the tip of a stainless steel capillary with an exterior diameter of 0.7 mm. A monolayer was deposited with a 0.5 μl syringe at the drop surface. The injected volume was usually 0.2 μl, varying between 0.1 and 0.4 μl. The lipid concentration was usually 0.2 mM. After deposition, the monolayer film pressure, Π was followed in time at a constant drop surface A. Once equilibrium was approached (i.e., $\Delta\Pi \leq 0.1$ mNm^{-1} within 5 min.), measurement of ε and η was started (i.e., Π of an oscillating drop was recorded). Data were analyzed with a Fourier transformation function for five periods. The drop oscillation was performed with the tensiometer automatic dosing system (Sinterface), which varied A following a sinusoidal function with a prescribed amplitude a_1 and frequency f.

The normalized amplitude a is as follows:

$$a = a_1/A_0 \times 100\,(\%). \quad (4)$$

From our previously published results (27), we decided to perform all rheological measurements presented here at a constant frequency $f = 18.2$ mHz. The amplitude a was chosen such that it allowed an optimized performance of the measurements, i.e., $a = 1.5\%$ for DPPC/cholesterol and DMPC/cholesterol mixtures and $a = 2.5\%$ for DOPC/cholesterol mixtures. It was impossible to use $a > 1.5\%$ for DPPC/cholesterol mixtures because higher amplitudes forced the drop to fall off at its minimum area and its corresponding minimum σ. In contrast, neither the elasticity ε of DOPC nor that of cholesterol changes when a is lowered from $a = 2.5\%$ to $a = 1.5\%$, as we demonstrated previously (27), with our data and in comparison with the results of Tournois et al. (23) who used $a \approx 1\%$ for DOPC. Therefore, the results produced for DOPC/cholesterol mixtures are fully comparable to those of mixtures of saturated phospholipids with cholesterol regarding their dynamic conditions.

RESULTS AND DISCUSSION

DPPC/cholesterol mixtures

Fig. 1 presents the surface rheology of DPPC/cholesterol monolayers with different amounts of cholesterol and a phase diagram summarizing phase transitions derived from breaks in ε and η. For DPPC/cholesterol mixtures, the cholesterol content x_C is varied between 0 and 100 mol % in seven steps (i.e., $x_C = 0$, 20, 40. 50, 60, 80, or 100 mol %). To simplify the notations used in the text and figures, the subscripts P, M, and O are used for DPPC/cholesterol, DMPC/cholesterol, and DOPC/cholesterol mixtures, respectively. The upper limit of film pressure for each experiment was monolayer collapse, i.e., multilayer formation or the pendent drop fell off due to the low surface tension.

The rheological data of DPPC/cholesterol mixtures are shown in Fig. 1, *A* and *C*, for ε_P and η_P, respectively. Fig. 1 *B* is an enlargement of the surface elasticity ε_P shown in Fig. 1 *A* to illustrate details at low ε_P. To document the reproducibility of ε_P and η_P, data of measurements with two independent drops are shown in Fig. 1, *A–C*, for all x_C-values using similar symbols for the duplicates as described in the figure legend. As can be seen, the ε_P and η_P curves can be divided into three linear segments of different slopes. Segment II is present only for $x_C \leq 40$ mol % and it appears as an intermediate plateau. The slopes m, ordinate intersections b, and the coefficients of

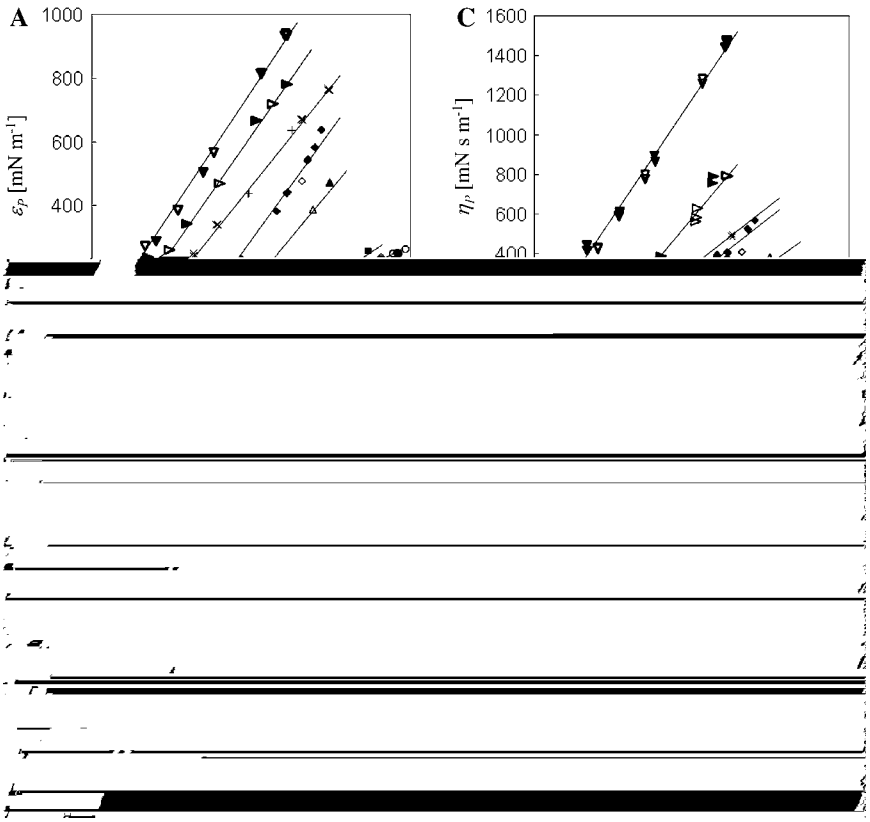

FIGURE 1 Surface elasticity ε_P, surface dilational viscosity η_P, and phase diagram of DPPC/cholesterol mixtures. (*A*) Surface elasticity ε_P versus Π; two measurements with independent drops are shown to document reproducibility; cholesterol content x_C: 0 mol % (25.3°C ± 0.2°C) (●, ○); 20 mol % (26.4°C ± 0.3°C) (■, □); 40 mol % (27.1°C ± 0.1°C) (▲, △); 50 mol % (28.8°C ± 0.4°C) (*solid diamonds*, *open diamonds*); 60 mol % (28.1 ± 0.1°C) (×, +); 80 mol % (27.3 ± 0.1°C) (*closed triangles and open triangles, both pointing to the right*); 100 mol % (26.2°C ± 0.2°C) (▼, ∇). (*B*) Magnification with respect to ε_P of data shown in Fig. 1 *A*. All solid inclined lines are linear regressions in the corresponding Π intervals; the plateau lines are arithmetic averages of the data points in that Π interval. The breaks in the solid curves are defined by intersection points between plateaus and linear regressions. Break points and linear regressions are shown in Table 1. (*C*) Surface dilational viscosity η_P corresponding to ε_P from Fig. 1 *A*. (*D*) Phase diagram presenting the phase transitions in the Π_P versus x_C plane. Breaks in the ε_P curves shown in Fig. 1, *A* and *B* (■). Breaks in the η_P curves shown in Fig. 1 *C* (*closed diamonds*). Phase boundaries stated by other authors, some of them not with DPPC, but similar fatty acids: Langmuir film balance measurements (9), DPPC/cholesterol, 24.9°C (*open diamonds*); Langmuir film balance measurements (37), DPPC/cholesterol, 21°C ± 2°C (○); fluorescence microscopy (41), DMPC/cholesterol 24.5°C ± 0.5°C (□); fluorescence microscopy (41), DiC15PC/cholesterol, 24.5°C ± 0.5°C (△).

correlation R^2 of the linear regressions of segments I and III are displayed in Table 1. The intermediate plateau is characterized by the mean value of either η_P or ε_P and its standard deviation (SD). In both segments I and III, the slopes increase with x_C. In segment III, the slopes are much higher than the respective slopes in segment I. The slopes in segment III are of the same order as the slope of the pure cholesterol curve. The extent of segment I decreases with increasing cholesterol content, and segment III begins at a smaller Π. The intersection points of the plateau with segments I and III are named transition points I and II, respectively; the intersection points between segments I and III are called transition points II. The latter are also shown in Table 1 with their respective film pressures Π. Fig. 1 *D* presents the phase transitions (i.e., transition points I and II in Table 1) of monolayers of DPPC/cholesterol mixtures displayed in a Π versus x_C diagram.

The results extracted from Fig. 1, *A* and *B*, were compared with those of other authors who were derived them either from isotherms on a Langmuir film balance (using monolayers in thermodynamic equilibrium) as previously reported (9,37) or from fluorescence microscopy (41). Our phase transition data are shown in Fig. 1 *D* as solid squares for ε_P from Fig. 1, *A* and *B*, and as solid diamonds for η_P, extracted from Fig. 1 *C*. Data from other authors are presented as open symbols in Fig. 1 *D*. All lines tentatively indicating phase boundaries in Fig. 1 *D* are only visual guides without an underlying theory. The regions separated by the phase boundaries are denoted (*i*) to (*vi*).

We will first focus on region (*i*) and the transition between it and region (*ii*) in Fig. 1 *D*. According to the micrographs shown in an article by Worthman et al.(37), dark domains form in region (*i*), which are surrounded by a continuous, bright monolayer phase for $0 \leq \Pi \leq 4$ mNm^{-1} and $10 \leq x_C \leq 30$ mol %. This description of region (*i*), which is usually referred to as the ''α-region'' of two separated liquid phases, was qualitatively confirmed by Stottrup et al. (3), where an α-region for $15 \leq x_C \leq 35$ mol % up to approximately $\Pi \approx 4$ mNm^{-1} was found. Unfortunately, their ternary DPPC/DOPC/cholesterol phase diagram does not allow the extraction of exact numbers for the transition between region (*i*) and (*ii*). Apparently, region (*i*) does not extend down to $x_C \rightarrow 0$ mol % because there are no domains visualized by micrographs for DPPC below $\Pi = 7.3$ mNm^{-1}. Furthermore, the transition between region (*i*) and (*ii*) cannot be monitored using static or dynamic surface elasticity as neither our results nor those demonstrated by Albrecht et al. (9) give an indication of this transition. The disappearance of the dark domains and the formation of a uniform liquid phase on transition from (*i*) to (*ii*) thus seems to have no mechanical consequences.

The transition from a uniform liquid phase in region (*ii*) to the two phase region (*iii*) is described by both dynamic and static elasticity measurements. In our measurements, shown in Fig. 1, *A*–C, this phase transition corresponds to a change from a linear increase of ε_P and η_P with Π to a plateau. Our phase boundary between (*ii*) and (*iii*) coincides well with a phase boundary as reported by Albrecht et al. (9), which these authors described as the ''liquidus line separating phases containing fluid DPPC from phases with crystalline lecithin.'' This phase transition between regions (*ii*) and (*iii*) can also be monitored using fluorescence microscopy. In Worthman et al.'s article (37), black domains are shown for DPPC/NBD-PC 99:1 mol % at $\Pi = 7.3$ and 10.1 mNm^{-1}, in the former case as a roughly circular domain, in the latter as an ''S'' shape. In the article by Stottrup and Keller (13), the black domain has a regular shape (like a ''curved tripod'') and is shown for DPPC/Texas Red-DPPE 99.5:0.5 mol % at $\Pi \approx 9$ mNm^{-1}. The authors described this phase separation as a ''solid domain in a background of a liquid phase.'' We can therefore conclude that, in region (*iii*), a continuous liq-

TABLE 1 Linear regressions of surface elasticity $\varepsilon_P(\Pi)$ and surface dilational viscosity $\eta_P(\Pi)$ in segments I–III, mean plateau values and transitions points (= curve breaks) I and II; measured data and regression lines shown in Fig. 1, *A–C*

x_C	Segment I			Segment II(plateau)	Segment III			Transition points	
Mol %	m	b	R^2	η_P or ε_P ($\pm$ SD)	m	b	R^2	I: Π	II: Π
Dilational viscosity $\eta_P(\Pi)$, measured data and regression lines shown in Fig. 1 *C*									
0	2.73	−5.4	0.916	45.0 ± 6.5	8.15	−167.6	0.973	18.2	26.0
20	2.57	7.3	0.692	39.5 ± 8.7	22.92	−564.4	0.929	12.5	26.3
40	5.43	4.4	0.989	64.6 ± 12.1	25.10	−493.1	0.931	11.0	22.3
50	6.99	18.3	0.971	–	27.31	−334.8	0.944	–	17.4
60	8.84	11.4	0.947	–	27.57	−284.4	0.999	–	15.8
80	9.36	69.4	0.972	–	41.98	−367.7	0.971	–	13.4
100	–	–	–	–	52.42	0	0.993	–	–
Dilational elasticity $\varepsilon_P(\Pi)$, measured data and regression lines shown in Fig. 1, *A* and *B*									
0	2.56	23.6	0.989	58.5 ± 2.1	11.91	−258.4	0.994	13.5	26.5
20	4.10	20.9	0.997	69.4 ± 6.1	14.98	−336.7	0.973	12.0	27.1
40	7.43	18.0	0.999	80.3 ± 2.9	26.66	−450.6	0.953	8.3	20.0
50	5.33	36.3	0.973	–	30.84	−403.7	0.976	–	17.3
60	13.75	16.1	0.977	–	27.95	−165.9	0.997	–	12.8
80	14.63	97.6	0.931	–	31.70	−94.3	0.994	–	11.3
100	–	–	–	–	33.32	6.7	0.995	–	–

uid phase and isolated solid aggregates coexist. Unfortunately, the fluorescence microscopy studies do not report about precise phase transition boundaries. From the micrographs shown in Nag et al.'s article (36), we can only extract the information that phase separation is not only visible for pure DPPC but also for DPPC/cholesterol mixtures above the α-region. For binary DPPC/cholesterol mixtures, Worthman et al. (37) demonstrated phase separation at ($x_C = 10$ mol %; $\Pi = 12.4$ mNm^{-1}) and ($x_C = 20$ mol %; $\Pi = 19.1$ mNm^{-1}). There is a discrepancy in the determination of the lower boundary of region (*iii*) for $x_C = 0$ mol % between fluorescence microscopy ($\Pi \approx 7.3$ mNm^{-1}) and the static or dynamic elasticity ($\Pi \approx 12$ mNm^{-1}). This discrepancy is assumed to be a specific effect of the fluorescent markers used. In fluorescence microscopy, it is of course impossible to study the phase behavior of ideally ''pure'' DPPC because of the use of fluorescent probes. von Tscharner and McConnell (50) demonstrated that even 1% of NBD-PE (*N*-(7-nitrobenz-2-oxa-1,3-diazol-4-yl)-1,2-dihexadecanoyl-*sn*-glycero-3-phosphoethanolamine) considerably changes the isothermal properties of a DPPC monolayer on a Langmuir film balance.

We summarize that, in region (*i*), condensed stoichiometric complexes of DPPC and cholesterol segregate from a second liquid phase rich in DPPC with higher solubility of the fluorescent probe. In region (*ii*), the condensed complexes re-dissolve, and only one homogeneous liquid phase prevails. In region (*iii*), Albrecht et al. noted that ''coexistence between a DPPC/cholesterol mixed phase and crystalline DPPC containing 2-5 mol % of cholesterol exists'' (9). Π/A isotherms show a plateau in Π at the lower bound of (*iii*) and a break in ε at the upper bound (9). Our results exhibit plateaus of both η and ε in the whole range of region (*iii*). This means that the transition from a liquid phase to solid DPPC domains in thermodynamic equilibrium results in a decrease of molecular area at constant Π mainly at the lower bound of region (*iii*), whereas dynamically this phase transition prohibits an increase of elasticity and dilational viscosity in the full range of (*iii*).

A phase boundary between region (*iii*) and (*iv*) was not explicitly described by Albrecht et al. (9), but it can be extracted as point ''K'' of their Fig. 3 and characteristic breaks in ε_P of their Fig. 4. Because ε_P and η_P increase linearly with Π in (*iv*) as shown in Fig. 1, *A–C*, and Table 1, we conclude that (*iv*) is a solid phase where compression leads to a linear increase of ε_P and η_P with Π. The upper bound of (*iv*), which is only described by Albrecht et al. (9) as the boundary beyond which ε_P becomes almost constant, is classified as a solid-solid transition by these authors.

The almost vertical phase boundary between regions (*i*) and (*iv*) on the left side and between (*v*) and (*vi*) on the right side is only described by Albrecht et al. (9) and by Worthman et al. (37) but closely corresponds to the stoichiometric ratio of 2:1, i.e., 33 mol % of cholesterol as described by others (44,47), although for $\Pi \leq 10$ mNm^{-1} the phase boundary between regions (*i*) and (*v*) is shifted to values where $x_C >$ 33 mol %. This phase boundary indicates the transition from films dominated by the DPPC content to films dominated by the cholesterol content as interpreted by Albrecht et al. (9). Region (*v*) is commonly referred to as the ''β-region,'' such as in the article by McConnell and Radhakrishnan (47).

For the transition between regions (*v*) and (*vi*), we could not find precise data produced by imaging methods of DPPC/cholesterol mixtures for comparison with our results. Unfortunately, neither Worthman et al. (37) nor Stottrup et al. (3) provided quantitative data of the upper limit of the β-region. Stottrup et al. only stated in the caption of their Fig. 4: ''Transition pressures in the β-region are greater than in the α-region, often well above 15 mNm^{-1}.'' They indicated measurements for binary DPPC/cholesterol mixtures for $x_C = 40$ and 45 mol % in their ternary phase diagram. Micrographs (37) reveal that the upper bound of the β-region is $>$12.0 mNm^{-1} for $x_C = 50$ mol % and $<$15.1 mNm^{-1} for $x_C = 80$ mol %. Thus, the studies by both Stottrup et al. (3) and Stottrup and Keller (13) are in qualitative agreement with the phase transition between regions (*v*) and (*vi*) found in this work, even though they cannot quantitatively support it. Therefore, we included phase transitions found for binary mixtures of dihydrocholesterol with either DMPC (consisting of 2 saturated fatty acids with 14 carbon atoms, i.e., 14:0;14:0) or DiC15 PC (15:0;15:0), the latter being homologous to DPPC (16:0; 16:0). Dihydrocholesterol yields the same phase diagrams as cholesterol (41). As can be seen in Fig. 1 *D*, the phase boundary between (*v*) and (*vi*) as given by Okonogi and McConnell (41) for DMPC/cholesterol and DiC15 PC/cholesterol is fairly close to the phase boundaries found here for η_P and ε_P. We therefore assume that a similar phase boundary can also be quantified for DPPC/cholesterol mixtures by fluorescence microscopy. It is interesting to note that Okonogi and McConnell (41) described the phenomenon of ''contrast inversion'' at this phase boundary when charged fluorescent probes are used but not for uncharged probes. According to these authors (41), the fluorescent probe accumulates in the condensed complex in the β-region (= region (*v*)), but probe solubility is inverted as Π is raised above the phase boundary with the probe accumulating in the cholesterol-rich phase in region (*vi*), whereas the geometry and position of the condensed complexes remain unchanged. When exposed to high Π, the condensed complexes may break up into smaller domains (41).

Okonogi and McConnell (41) also postulated that both (*v*) and (*vi*) are two phase regions. As shown in Fig. 1, *A–C*, passing the boundary between (*v*) and (*vi*) is accompanied by a break in the η_P and ε_P curves, which increases to approximately the same rate as the curve of pure cholesterol in (*vi*). It has been shown statistically (37) and visually (41) that the area ratio of the domains and the surrounding phase remains constant for $x_C > 30$ mol % for all Π. Therefore, it can be concluded that, in region (*v*), the condensed stoichiometric complexes containing 66 mol % of DPPC dominate the rheological properties whereas, in (*vi*), the rheology of the condensed complexes has adapted to that of the cholesterol-

rich phase that dominates η and ε. In other words, the molecular interactions within the condensed complexes in (*v*) are similar to those of pure DPPC, whereas they are more similar to pure cholesterol in (*vi*). Apparently, this change of interactions is accompanied by an inversion of solubility of the fluorescent probe Texas-Red-DHPE (41). It is interesting that the phase transition from (*v*) to (*vi*) cannot be detected by measuring the surface elasticity statically, as there are no breaks visible in the Π/A-isotherms in the work by Albrecht et al. (9). In contrast, a very prominent change can be visualized using dynamic surface elasticity as shown here.

Because no accurate data for the phase transition between regions (*v*) and (*vi*) could be found in the literature for DPPC/cholesterol mixtures, we decided to include the DMPC/cholesterol system into our study, which will be presented in the following section.

DMPC/cholesterol mixtures

As the gel/liquid crystalline main phase transition for DMPC in a bilayer state occurs at room temperature, i.e., $T_m = 23.5°C$, we decided to perform all measurements with DMPC in a thermostated measurement chamber. In Fig. 2 *A*, we show the surface elasticity ε_M versus Π at $T = 20 \pm 0.1°C$, and an enlargement with respect to ε_M is illustrated in Fig. 2 *B*. To gain a good resolution for the phase diagram shown in Fig. 3, we changed the cholesterol content for the DMPC system by steps of 10 mol % with a total of eight steps for $x_C = 0$ to 70 mol % plus pure cholesterol, i.e., $x_C = 100$ mol %. To account for temperature effects, we varied T in three steps, i.e., $T = 20°C$, 25°C, and 30°C. A representative selection of mixtures is shown in Fig. 2 *C* for all three temperatures and the mixtures $x_C = 0$, 40, 50, 60, and 100 mol %. An enlargement of Fig. 2 *C* with respect to ε_M is shown in Fig. 2 *D*. As the dilational viscosity η_M does not provide additional information about phase separations and transitions, we only show and discuss ε_M and not η_M. Similar to the DPPC/cholesterol system, all curves are divided into linear segments. The slopes m, ordinate intersections b, and the coefficients of correlation R^2 of the linear regressions of segments I–III are provided in Table 2 for all curves shown in Fig. 2. In all cases where an intermediate horizontal plateau is found, this is characterized by the mean value of $\varepsilon_M \pm$ its SD.

In the next section, we focus on the qualitative differences of the DMPC curves shown in Fig. 2 compared to those of DPPC in Fig. 1. As can be seen in Fig. 2, *B* and *D*, in some curves the ''breaks'' between segment II and III are ''smoothed,'' i.e., the data points describe a finite curvature instead of an ideal break. In these cases, particularly for 20 and 30 mol % in Fig. 2 *B* and for 40 mol %, 25°C and 30°C, in Fig. 2 *D*, some data points (maximally $\pm$ 5 mNm^{-1} around an interpolated break) were ignored for the evaluation of either trendlines or horizontal plateaus. We interpret this effect of smoother phase transitions for DMPC than for DPPC as being due to the fact that measurements were taken around T_m for DMPC ($T_m = 23.5°C$) but at much lower temperatures

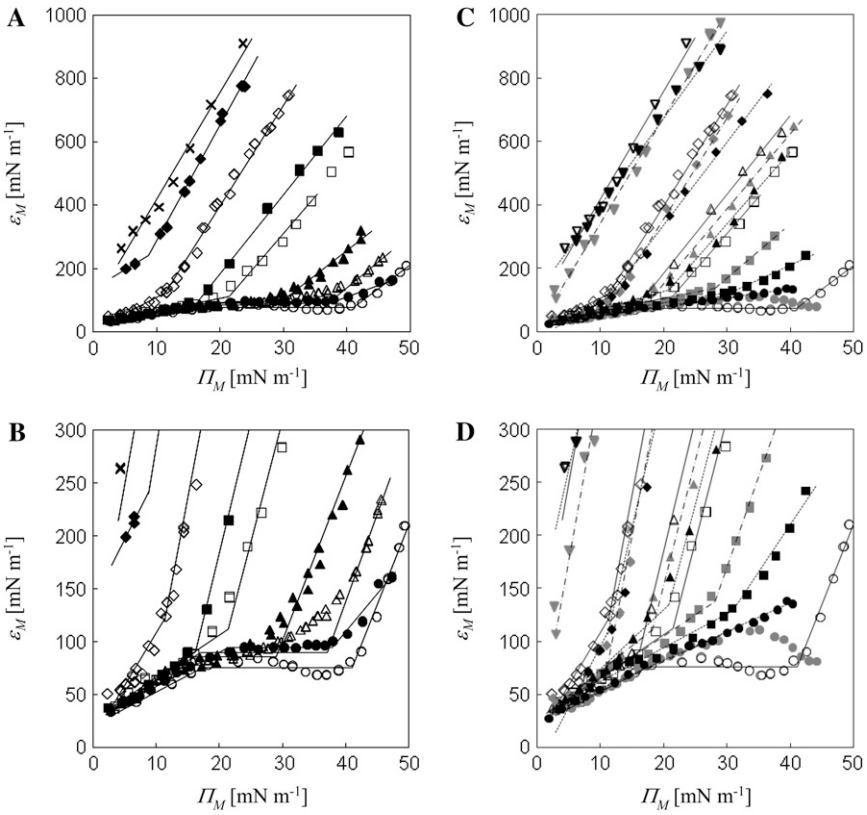

FIGURE 2 Surface elasticity ε_M of DMPC/cholesterol mixtures. (*A*) ε_M versus Π at 20°C $\pm$ 0.1°C, cholesterol content x_C: 0 mol % (○); 10 mol % (●); 20 mol % (△); 30 mol % (▲); 40 mol % (□); 50 mol % (■); 60 mol % (*open diamonds*); 70 mol % (*solid diamonds*); 100 mol % (×). (*B*) Magnification with respect to ε_M of data shown in Fig. 2 *A*. The lines represent linear regressions, see Fig. 1 legend. (*C*) Surface elasticity ε_M versus Π at three temperatures: 20°C (*open circles, squares, upward triangles, diamonds, downward triangles*); 25°C (*gray circles, squares, upward triangles, diamonds, downward triangles*); and 30°C (*black circles, squares, upward triangles, diamonds, downward triangles*); for some DMPC/cholesterol mixtures: 0 mol % (○, *gray circle*, *solid circle*); 40 mol % (□, *gray square*, ■); 50 mol % (△, *gray triangle*, ▲); 60 mol % (*open diamonds, gray diamonds, solid diamonds*); 100 mol % (∇, *gray downward triangle*, ▼). (*D*) Magnification with respect to ε_M of data shown in Fig. 2 *C*.

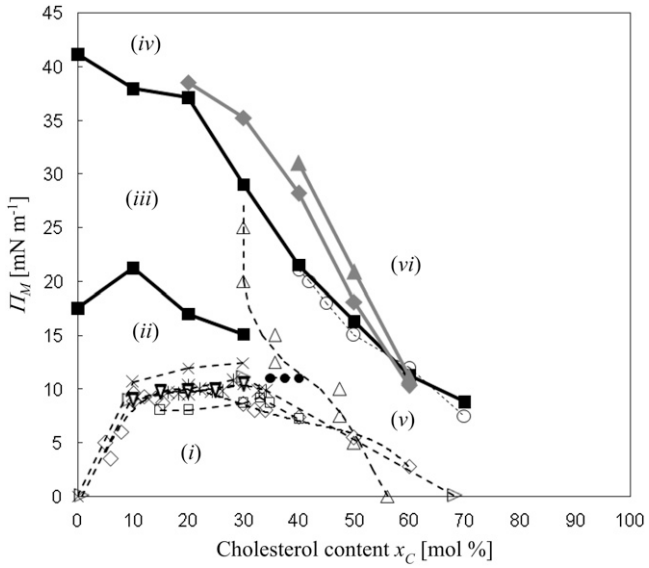

FIGURE 3 Phase diagrams of DMPC/cholesterol mixtures in the Π_M versus x_C plane. Breaks in the ε_M curves shown in Fig. 2, *A* and *B*, at 20°C; breaks in the ε_M curves at 25°C and 30°C, respectively (*gray diamonds, gray triangles*). Phase boundaries stated by other authors with epifluorescence microscopy: Keller et al. (39) 23°C ± 0.5°C (*open diamonds*, *stars*); Okonogi and McConnell (41), 24.5°C ± 0.5°C (○, ●, ∇); Hirshfeld and Seul (15), 23.5°C (△); Subramaniam & McConnell (14), 25°C ± 1°C (×); Benvegnu and McConnell (16), room temperature (□, *open triangle pointing to the right*).

for DPPC ($T_m = 41$°C). Another difference regarding DPPC is that there are two curves where data points decrease with growing Π, which take place for pure DMPC at 20°C and 25°C. In the case of the 20°C curve, the averaged horizontal plateau seems to have a shallow local maximum and minimum; the 25°C curve seems to decline above 33 mNm^{-1}; we assume the latter, however, to be an artifact produced, for example, by multilayer formation.

When focusing on the phase diagram for the DMPC/cholesterol mixtures shown in Fig. 3, six regions can be distinguished, similar to Fig. 1 *D*. However, the phase transition boundaries in the range $0 \leq x_C \leq 40$ mol % are shifted to a higher Π compared to Fig. 1 *D*. As for DPPC/cholesterol mixtures, the upper bound of region (*i*) (which is identical to the α-region) can only be proven by using fluorescence microscopy. In the $15 \leq x_C \leq 35$ mol % range, shape transitions and the appearance of a stripe phase has been reported at the upper boundary of region (*i*) (16,39). Region (*ii*) is reported to be a homogeneous liquid phase. Unfortunately, very little quantitative data are provided by other authors for the transition from region (*ii*) to (*iii*). This is because fluorescence microscopy has usually been conducted at room temperature, i.e., 23°C ± 0.5°C (39), where a solid /liquid phase coexistence or even transition to a single solid phase are no longer visible. However, there are very valuable data for pure DMPC that quantitatively support the data presented here for the lower and upper bounds of region (*iii*). Measuring isobars on a Langmuir trough in thermodynamic equilibrium, Blume shows (see Fig. 2 in his article) (10) that DMPC monolayers at $15 \leq \Pi \leq 35$ mN^{-1} (measured in steps of +5 mNm^{-1}) exist in three different phases in the temperature range of 5°C $\leq T \leq 35$°C. At the low temperatures of phase A, the molecular area A_{mol} is constant with respect to temperature; at the intermediate temperatures of phase B, it increases strongly; at the higher temperatures of phase C, it increases weakly. At 20°C, the monolayer is at 15 mNm^{-1} in phase C and at $20 \leq \Pi \leq 35$ mNm^{-1} in phase B. The transition to phase A can be extrapolated from Blume's data (10) to take place in the 35–40 mNm^{-1} range. If we identify phase C to be our region (*ii*), phase B region (*iii*), and phase A region (*iv*), there is good quantitative agreement between static isobars and our dynamic elasticity results. The lower and upper bound of region (*iii*) are 17.5 and 41.1 mNm^{-1} for $x_C = 0$ mol %, respectively, in coincidence with the bounds of phase B as described by Blume (10). Further, our results are qualitatively confirmed by atomic force microscopy micrographs as reported by Sardone (11) who shows homogeneous phases in the low and high Π ranges and domain formation in between. Sardone (11), however, renders no data for the phase transitions.

Concerning phase transitions of pure DMPC, we state that both dynamic elasticity results and static Langmuir isobars appear more suitable for the detection of precise phase transitions than static Langmuir isotherms. DMPC isotherms only possess a plateau at low T (11)) from which the lower bound of region (*iii*) can be deduced, whereas the upper bound is seen as a break in the isotherm. At higher T-values, the plateau is more and more smoothed, which makes it impossible to extract phase transition values. From our own results for DMPC, the cited literature, and a comparison to the results presented for DPPC, we conclude the following: Region (*ii*) is a homogeneous liquid phase where ε_M is linearly increasing with Π and where A_{mol} is weakly increasing with T. In region (*iii*), coexistence of a liquid and a solid phase occurs, where ε_M is independent of Π, and A_{mol} strongly increases with T. Region (*iv*) is a homogeneous solid phase, where ε_M is linearly and strongly increasing with Π and where A_{mol} is independent of T.

A phase transition able to discriminate regions (*i*) – (*iv*) in the low x_C range from regions (*v*) – (*vi*) in the high x_C range has been reported by Hirshfeld and Seul (15), where it could be deduced from static Langmuir isobars in a x_C versus ε_M plot. Their curve qualitatively coincides with a similar phase boundary reported for DPPC (9,37). In the high Π range, this phase boundary is vertical with a value of $x_C \approx 33$ mol %; at low Π, it intersects the upper bound of the α-region reported previously (16,39). The existence of a β-region for DMPC was only reported by Okonogi and McConnell (41) after the publication of articles by Hirshfeld and Seul (15) and Radhakrishnan and McConnell (38). Okonogi and McConnell (41) stated that a β-region must have been overlooked in these earlier studies and, at the same time, corrected the extent of the

TABLE 2 Linear regressions of dilational elasticity $\varepsilon_M(\Pi)$, in segments I–III, mean plateau values and transitions points (= curve breaks) I and II; measured data and regression lines shown in Fig. 2, *A–D*

x_C	Temp	Segment I			Segment II	Segment III			Transition points	
mol %	[°C]	m	b	R^2	ε_M (± SD)	m	B	R^2	I: Π	II: Π
0	20	3.14	20.6	0.999	75.7 ± 5.5	15.15	−547.1	0.970	17.5	41.1
0	25	2.74	25.8	0.972	–	–	–	–	–	–
0	30	2.71	27.7	0.992	–	–	–	–	–	–
10	20	3.24	25.3	0.993	91.6 ± 2.5	7.26	−181.4	0.933	21.2	37.9
20	20	3.84	23.9	0.994	89.6 ± 6.7	16.64	−527.3	0.993	17.0	37.1
20	25	1.53	37.2	0.997	–	10.25	−298.4	0.999	–	38.5
20	30	–	–	–	–	2.48	26.6	0.995	–	–
30	20	4.30	20.5	0.980	85.2 ± 7.7	15.52	−364.6	0.951	15.1	29.0
30	25	2.35	28.7	0.951	–	14.97	−415.7	0.985	–	35.2
30	30	2.83	26.9	0.916	–	–	–	–	–	–
40	20	4.03	25.7	0.954	–	23.21	−385.8	0.986	–	21.5
40	25	4.03	23.9	0.975	–	17.23	−347.8	0.994	–	28.2
40	30	3.20	29.3	0.974	–	9.08	−152.9	0.968	–	31.0
50	20	4.19	22.5	0.976	–	24.86	−313.7	0.995	–	16.2
50	25	4.71	24.9	0.941	–	23.48	−316.0	0.993	–	18.1
50	30	5.61	17.4	0.972	–	22.70	−339.9	0.985	–	20.9
60	20	10.09	7.3	0.910	–	31.81	−240.4	0.989	–	11.3
60	25	1.11	43.2	0.999	–	31.64	−275.2	0.997	–	10.3
60	30	11.60	-21.2	0.984	–	26.16	−186.5	0.992	–	11.2
70	20	11.88	137.0	0.947	–	36.52	-81.2	0.994	–	8.8
100	20	–	–	–	–	33.88	78.7	0.983	–	–
100	25	–	–	–	–	33.32	6.7	0.995	–	–
100	30	–	–	–	–	27.46	123.7	0.993	–	–

α-region to $x_C \leq 40$ mol %, which is no longer in conflict with the phase boundary given by Hirshfeld and Seul (15).

The phase transition between regions (*v*) and (*vi*) found here for $T = 20$°C matches very well with the values given by Okonogi and McConnell (41) for the contrast inversion pressure (discussed previously in the section, ''DPPC/cholesterol mixtures'') at $T = 24.5$°C ± 0.5°C in the range of $x_C = 40$–70 mol %. We will first focus on the nature of this phase transition and then discuss temperature effects. What is the physical state of the mixed monolayer in region (*vi*)? As previously mentioned in the section, ''DPPC/cholesterol mixtures,'' Okonogi and McConnell (41) described the persistence of domains upon transition from (*v*) to (*vi*). For charged probes, they discovered the phenomenon of ''contrast inversion,'' meaning that a bright domain with a dark background in (*v*) turned dark with a brighter background upon transition to (*vi*). They interpreted the bright domains in (*v*) to be poor in cholesterol. Uncharged probes never inverted the contrast of the domains but, in some cases, domains disappeared upon transition from (*v*) to (*vi*) and reappeared within region (*vi*) at higher Π. From these facts, the authors concluded that both regions (*v*) and (*vi*) are two phase regions (41). Our elasticity data ε_M describe the mechanical properties of the monolayers in both regions. As can be seen in Fig. 2 and Table 2, ε_M increases weakly with Π with a growth rate $\partial\varepsilon_M/\partial\Pi \approx 5$ in region (*v*). In contrast, the growth rate $\partial\varepsilon_M/\partial\Pi$ is between 17 and 33 in region (*vi*). The growth rate $\partial\varepsilon_M/\partial\Pi$ is thus higher in region (*vi*) than in region (*iv*), which is interpreted as a solid phase. Therefore, we interpret region (*vi*) to consist of two solid-like separated phases. The question remains whether there is any difference between regions (*iv*) and (*vi*). Both appear to be solid-like, but this has to be clarified using imaging methods whether (*iv*) is constituted by a single homogeneous or two separated solid phases.

We will now discuss the temperature effects seen in Fig. 3. The most prominent effect is that there is no phase transition between regions (*ii*) and (*iii*) and between regions (*iii*) and (*iv*) for $T = 25$°C and 30°C, except for $x_C = 20$ and 30 mol % at $T = 25$°C. This means that a transition to a coexistence of a fluid and a solid phase (taking place in (*iii*) at low T) does not occur for at $T \geq 25$°C. Similarly, a transition to a solid phase (taking place in (*iv*) at low T) does not occur at $T \geq 30$°C. Yet, it does occur for $x_C = 20$ and 30 mol % at $T = 25$°C. This means that the main transition $T_m = 23.5$°C is increased to higher T by the presence of cholesterol. For $x_C = 20$–50 mol %, the phase transitions measured for $T = 25$°C and 30°C are higher than those at $T = 20$°C. At $x_C = 60$ mol %, however, there is no difference in the phase transition pressures between region (*v*) and (*vi*). This seems to be related to the fact that, within experimental errors, the dynamic elasticity ε of pure cholesterol is independent of T (Fig. 2 *C*).

DOPC/cholesterol mixtures

The rheological data of DOPC are shown in Fig. 4. Globally, all curves of ε_O and η_O can be roughly characterized by single linear regressions as shown in Fig. 4, *A* and *C*. Here, phase

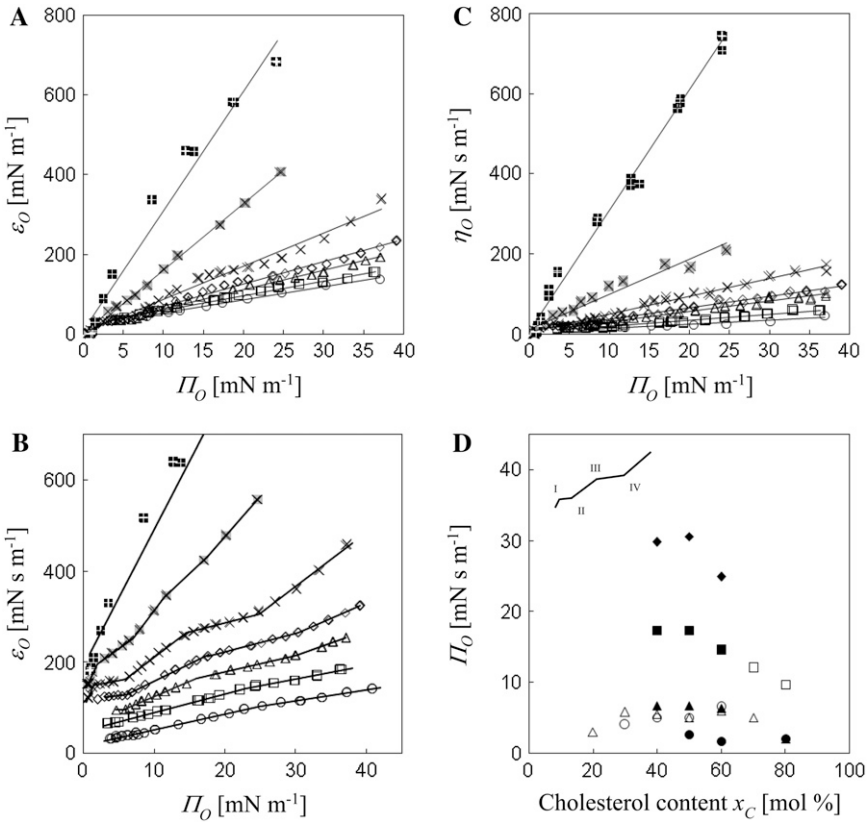

FIGURE 4 Surface elasticity ε_O, surface dilational viscosity η_O, and phase diagram of DOPC/cholesterol mixtures. (*A*) Surface elasticity ε_O versus Π for different cholesterol contents: 0 mol % (22.3°C) (○); 20 mol % (26.0°C) (□); 40 mol % (27.5°C) (△); 50 mol % (27.5°C) (*open diamonds*); 60 mol % (26.8°C) (×); 80 mol % (26.0°C) (*gray squares* with ×); 100 mol % (26.2°C) (*solid squares* with *white* +). The lines represent linear regressions, see Fig. 1 legend. (*B*) Magnification with respect to ε_O of data shown in Fig. 4 *A*. The curves are separated by adding $n \times (+ 30$ mN m$^{-1})$, $n = 1, 2, 3, \ldots$ in ascending order of x_C to ensure a better distinction of data. (*C*) Surface dilational viscosity η_O versus Π, symbols for different x_C as in Fig. 4, *A* and *B*. (*D*) Phase diagram presenting the phase transitions in the Π_O versus x_C plane. Breaks in the curves are denoted by I, II, III, and IV as shown in the schematic insert. Break I (●); break II (▲); break III (■); break IV (*solid diamonds*). Phase boundaries stated by other authors for DOPC/cholesterol mixtures using fluorescence microscopy: Okonogi and McConnell (41), 24.5°C ± 0.5°C (○, □); Hagen and McConnell (40), 21°C ± 1°C (△).

transitions are much less prominent than for ε_P, ε_M, and η_P. The slopes of the ε_O and η_O curves for $0 \leq x_C \leq 60$ mol % only slightly increase with x_C, but they are still much more similar to those of pure DOPC than to those of pure cholesterol. For $x_C = 80$ mol %, the slope is considerably augmented compared to $x_C \leq 60$ mol %, but they are still clearly smaller than for pure cholesterol. To better reveal the details of Fig. 4 *A*, the curves are shown in staggered arrangement in ascending order of x_C in Fig. 4 *B*, with each successive curve (from $x_C = 0$ to 100 mol %) being shifted by $+30$ mNm^{-1}. This presentation shows breaks in some curves indicating phase transitions. The breaks between linear segments of the ε_O curves are classified I to IV as shown by the schematic insert in Fig. 4 *D*. In the cases $x_C = 50$ and 60 mol %, a plateau appears between break I and II. Our rheological data (breaks I–IV) are denoted with filled symbols in Fig. 4 *D* as given in the figure legend. For comparison, the upper bounds of two immiscible liquid phases as revealed by fluorescence microscopy are represented by open spheres (as given by Okonogi and McConnell (41)) or open triangles (as presented by Hagen and McConnell (40)). Open squares indicate a phase boundary where contrast inversion of the fluorescent probe was observed in the article by Okonogi and McConnell (41), which only occurred for 70 and 80 mol % cholesterol. In that article, it was also reported that contrast inversion was only observed in the β-region, whereas the region adjacent to the α-region at higher Π was a homogeneous phase. It can therefore be concluded that the stoichiometric mixture of condensed DOPC/cholesterol complexes consists of x_C ~60–70 mol % of cholesterol.

There is very good agreement between break II and the upper bound of the α-region for $x_C = 40$, 50, and 60 mol %. In Fig. 4 *B*, there is a (short) plateau between breaks I and II for $x_C = 50$ and 60 mol %, which indicates a coexistence of two phases. The upper bound of the α-region is the limit where all domains have disappeared (41). The plateau shown in dynamic measurements of ε_O can therefore be interpreted as a coexistence region of the two immiscible phases (as described by fluorescence microscopy for the α-region). Above the α-region, only a single phase remains visible by fluorescence microscopy (41). It appears worth noting that for DOPC/cholesterol mixtures the upper bound of the α-region can be detected both by fluorescence microscopy and by dynamic elasticity measurements whereas, for the mixtures of DPPC and DMPC with cholesterol, it can only be detected with imaging methods.

Break III marks a decrease of the slope for $x_C = 40$–60 mol %. Okonogi and McConnell (41) reported that the boundary of contrast inversion was in the same range, but only for $x_C = 70$ and 80 mol %. Therefore, it is unclear if this decrease in the growth rate for ε_O corresponds to the phenomenon of contrast inversion. As discussed previously, contrast inversion for DMPC/cholesterol mixtures corresponds to a pronounced increase in the growth rate of ε_M. Break IV,

which indicates the transition to an increased growth rate of ε_O, can only be seen for some of the mixtures; it is most pronounced for $x_C = 60$ mol %. But, as there is no phase transition in that range reported for imaging methods, there is no basis as yet for a physical interpretation.

Although the phase boundary for contrast inversion is not reflected by breaks of growth rates in the ε_O curves, Fig. 4, *A* and *B*, clearly show that the global slope of the ε_O and η_O curves for $x_C \geq 80$ mol % are much higher, whereas those for $x_C \leq 60$ mol % are lower. It is assumed that, for $x_C \leq 60$ mol %, an α-region exists for low Π where the condensed complexes separate from a phase that is rich in DOPC whereas, for $x_C > 60$ mol %, they separate from a phase that is rich in cholesterol. Because the molar composition of the condensed complexes is constant for all mixtures, the local rheological properties of the complexes are equal for all mixtures. Thus, the second phase, immiscible with the condensed complexes, determines the global rheology of the monolayers, which is expressed in a rise of the growth rate for ε_O between $x_C = 60$ and 80 mol %. Therefore, our rheological data quantitatively support the distinction of an α- and a β-region in DOPC/cholesterol mixtures as described by Okonogi and McConnell (41).

CONCLUSIONS

It was demonstrated that the increase of the surface dilational viscosity η with film pressure Π parallels that of surface elasticity ε for DPPC/cholesterol and DOPC/cholesterol mixtures.

For binary mixtures of the saturated lipids DPPC and DMPC with cholesterol, six distinct regions could be found in a film pressure Π versus cholesterol content x_C phase diagram. The phase boundaries found here are in good agreement with phase transitions reported in the literature for static rheological measurements (i.e., isotherms and isobars on a Langmuir trough) and imaging methods (fluorescence microscopy and atomic force microscopy). Imaging shows the separation of two liquid phases with circular domains at low cholesterol contents x_C, the so-called ''α-region''. The domains disappear at higher Π, and a single fluid phase remains. Formation and disappearance of separated liquid phases in the α-region have no consequences on the mechanical properties of the monolayers. At higher Π and low x_C, for DPPC approximately $\Pi \approx 10$ mNm^{-1}, for DMPC at $\Pi = 15$–0 mNm^{-1}, all methods indicate coexistence of a liquid and a solid phase as described by Albrecht et al. (9) up to $\Pi \approx 25$ mNm^{-1} (for DPPC) or $\Pi \approx 35$ mNm^{-1} (for DMPC). Above, the monolayer is in a solid state, for which a linear growth rate of ε_P, ε_M, and η_P is found. A solid-solid phase transition was reported to occur at $\Pi \approx 38$ mNm^{-1} (9).

For $x_C \geq 40$ mol %, only one break occurs in the growth rate of ε_P, ε_M, and η_P. Above this phase transition, the growth rate is of the same order as that of pure cholesterol. Imaging methods report an inversion of contrast of the domains and their surrounding phase around this phase boundary. It is assumed that, below this transition, interactions within the condensed complexes are similar to those of the phospholipid, whereas above this they are more similar to pure cholesterol. This phase transition cannot be shown by static surface rheology; it is only revealed by imaging and dynamic surface rheology. This phase boundary is the upper bound of the so-called ''β-region''.

DOPC/cholesterol mixtures generally possess much smaller growth rates of η_O and ε_O with Π, which are all roughly linear. Only a more detailed analysis reveals breaks of the curves, especially for $x_C = 40$–80 mol %. At low Π, a short plateau becomes visible in that x_C-range that coincides with a so-called ''α-region'' of condensed stoichiometric complexes separated from a phase that is rich in DOPC. Interestingly, dynamic elasticity measurements are capable of detecting the α-region for an unsaturated lipid, but that is not the case for the saturated lipids DPPC and DMPC in their mixtures with cholesterol. The only clear indication of a β-region where the condensed complexes are separated from a phase rich in cholesterol is given by the fact that the growth rate of ε_O and η_O is considerably increased for $x_C \geq 80$ mol % compared to $x_C \leq 60$ mol %.

We are indebted to the referees for their competent criticisms and helpful advice. We thankfully acknowledge technical assistance rendered by S. Nikolaus and P. Wandrés, and part of the measurements being performed by Walter Oswald.

The DMPC was a gift from Lipoid (Ludwigshafen, Germany), and funding was provided by the Deutsche Forschungsgemeinschaft (DFG), LE 1119/3-1,2.

REFERENCES

1. McIntosh, T. J., A. Vidal, and S. A. Simon. 2003. Sorting of lipids and transmembrane peptides between detergent-soluble bilayers and detergent-resistant rafts. *Biophys. J.* 85:1656–1666.
2. Veatch, S. L., and S. L. Keller. 2002. Organization in lipid membranes containing cholesterol. *Phys. Rev. Lett.* 89:2681011–2681014.
3. Stottrup, B. L., D. S. Stevens, and S. L. Keller. 2005. Miscibility of ternary mixtures of phospholipids and cholesterol in monolayers, and application to bilayer systems. *Biophys. J.* 88:269–276.
4. Yan, W., B. Piknova, and S. B. Hall. 2005. The collapse of monolayers containing pulmonary surfactant phospholipids is kinetically determined. *Biophys. J.* 89:306–314.
5. Ma, G., and H. C. Allen. 2006. DPPC Langmuir monolayer at the air-water interface: probing the tail and head groups by vibrational sum frequency generation spectroscopy. *Langmuir.* 22:5341–5349.
6. Pawelec, M. K., and T. R. Sosnowski. 2003. Langmuir-Wilhelmy balance studies of DPPC and CTAB films. *In* Surfactants and Dispersed Systems in Theory and Practice. K. A. Wilk, editor. Oficyna Wyd. Polit. Wroc., Wroclaw. 267–270.
7. Pawelec, M. K., and T. R. Sosnowski. 2003. Relaxation phenomena at the air-water interface with surfactants. *Applied Mechanics and Engineering.* 8:295–300.
8. Wüstneck, R., N. Wüstneck, D. O. Grigoriev, U. Pison, and R. Miller. 1999. Stress relaxation behaviour of dipalmitoyl phosphatidylcholine monolayers spread on the surface of a pendant drop. *Colloids Surf. B.* 15:275–288.

9. Albrecht, O., H. Gruler, and E. Sackmann. 1981. Pressure-composition phase diagrams of cholesterol/lecithin, cholesterol/phosphatidic acid, and lecithin/phosphatidic acid mixed monolayers: a Langmuir film balance study. *J. Colloid Interface Sci.* 79:319–338.
10. Blume, A. 1979. A comparative study of the phase transitions of phospholipid bilayers and monolayers. *Biochim. Biophys. Acta.* 557:32–44.
11. Sardone, L. 2005. Nanostructured molecular films with functional applications for supramolecular electronics. PhD thesis. Louis Pasteur University, France.
12. Gaboriaud, F., R. Volinsky, A. Bermana, and R. Jelineka. 2005. Temperature dependence of the organization and molecular interactions within phospholipid/diacetylene Langmuir films. *J. Colloid Interface Sci.* 287:191–197.
13. Stottrup, B. L., and S. L. Keller. 2006. Phase behavior of lipid monolayers containing DPPC and cholesterol analogs. *Biophys. J.* 90:3176–3183.
14. Subramaniam, S., and H. M. McConnell. 1987. Critical mixing in monolayer mixtures of phospholipid and cholesterol. *J. Phys. Chem.* 91:1715–1718.
15. Hirshfeld, C. L., and M. Seul. 1990. Critical mixing in monomolecular films: pressure-composition phase diagram of a two-dimensional binary mixture. *J. Phys. France.* 51:1537–1552.
16. Benvegnu, D. J., and H. M. McConnell. 1993. Surface dipole densities in lipid monolayers. *J. Phys. Chem.* 97:6686–6691.
17. Ratajczak, M. K., Y. T. C. Ko, Y. Lange, T. L. Steck, and K. Y. C. Lee. 2007. Cholesterol displacement from membrane phospholipids by hexadecanol. *Biophys. J.* 93:2038–2047.
18. Kretzschmar, G., J. Li, R. Miller, H. Motschmann, and H. Mohwald. 1996. Characterisation of phospholipid layers at liquid interfaces. 3. Relaxation of spreading phospholipid monolayers under harmonic area changes. *Colloids Surf. A.* 114:277–285.
19. Yun, H., Y.-W. Choi, N. J. Kim, and D. Sohn. 2003. Physicochemical properties of phosphatidylcholine (PC) monolayers with different alkyl chains, at the air/water interface. *Bull. Korean Chem. Soc.* 24:377–383.
20. Li, J. B., J. Krägel, A. V. Makievski, V. B. Fainermann, R. Miller, and H. Möhwald. 1998. A study of mixed phospholipid/β-casein monolayers at the water/air surface. *Colloids Surf. A.* 142:355–360.
21. Krägel, J., G. Kretzschmar, J. B. Li, G. Loglio, R. Miller, and H. Möhwald. 1996. Surface rheology of monolayers. *Thin Solid Films.* 284–285:361–364.
22. Krägel, J., J. B. Li, R. Miller, M. Bree, G. Kretzschmar, and H. Möhwald. 1996. Surface viscoelasticity of phospholipid monolayers at the air/water interface. *Colloid Polym. Sci.* 274:1183–1187.
23. Tournois, H., P. Gieles, R. Demel, J. de Gier, and B. de Kruijff. 1989. Interfacial properties of gramicidin and gramicidin-lipid mixtures measured with static and dynamic monolayer techniques. *Biophys. J.* 55:557–569.
24. Miller, R., N. Wüstneck, J. Krägel, and G. Kretzschmar. 1996. Dilational and shear rheology of adsorption layers at liquid interfaces. *Colloids Surf. A.* 111:75–118.
25. Li, J., R. Miller, and H. Möhwald. 1996. Phospholipid monolayers and their dynamic interfacial behaviour studied by axisymmetric drop shape analysis. *Thin Solid Films.* 284–285:357–360.
26. Li, J., R. Miller, and H. Möhwald. 1996. Characterisation of phospholipid layers at liquid interfaces. 2. Comparison of isotherms of insoluble and soluble films of phospholipids at different fluid/water interfaces. *Colloids Surf. A.* 114:123–130.
27. Vrânceanu, M., K. Winkler, H. Nirschl, and G. Leneweit. 2007. Surface rheology of monolayers of phospholipids and cholesterol measured with axisymmetric drop shape analysis. *Colloids Surf. A.* 311:140–153.
28. Wüstneck, R., P. Enders, N. Wüstneck, U. Pison, R. Miller, and D. Vollhardt. 1999. Surface dilational behaviour of spread dipalmitoyl phosphatidyl glycerol monolayers. *PhysChemComm.* 2:50–61.
29. Loglio, G., P. Pandolfini, R. Miller, A. V. Makievski, R. Ravera, M. Ferrari, and L. Liggieri. 2001. Drop and bubble shape analysis as a tool for dilational rheological studies of interfacial layers. *In* Novel Methods to Study Interfacial Layers (Studies in Interface Science). R. Miller, editor. Elsevier, Amsterdam. 439–485.
30. Li, J., R. Miller, D. Vollhardt, and H. Möhwald. 1998. Spreading concentration effect on the morphology of phospholipid monolayers. *Thin Solid Films.* 327–329:84–86.
31. Li, J., R. Miller, R. Wüstneck, H. Möhwald, and A. W. Neumann. 1995. Use of pendent drop technique as a film balance at liquid/liquid interfaces. *Colloids Surf. A.* 96:295–299.
32. Saulnier, P., F. Boury, A. Malzert, B. Heurtault, T. Ivanova, A. Cagna, I. Panaiotov, and J. Proust. 2001. Rheological model for the study of dilational properties of monolayers. Comportment of dipalmitoylphosphatidylcholine (DPPC) at the dichloromethane (DCM)/water interface under ramp type or sinusoidal perturbations. *Langmuir.* 17:8104–8111.
33. Wüstneck, N., R. Wüstneck, V. B. Fainerman, R. Miller, and U. Pison. 2001. Interfacial behaviour and mechanical properties of spread lung surfactant protein/lipid layers. *Colloids Surf. B.* 21:191–205.
34. Crane, J. M., G. Putz, and S. B. Hall. 1999. Persistence of phase coexistence in disaturated phosphatidylcholine monolayers at high surface pressures. *Biophys. J.* 77:3134–3143.
35. Discher, B. M., W. R. Schief, V. Vogel, and S. B. Hall. 1999. Phase separation in monolayers of pulmonary surfactant phospholipids at the air-water interface: composition and structure. *Biophys. J.* 77:2051–2061.
36. Nag, K., and K. M. W. Keough. 1993. Epifluorescence microscopic studies of monolayers containing mixtures of dioleoyl- and dipalmitoylphosphatidylcholines. *Biophys. J.* 65:1019–1026.
37. Worthman, L. A. D., K. Nag, P. J. Davis, and K. M. W. Keough. 1997. Cholesterol in condensed and fluid phosphatidylcholine monolayers studied by epifluorescence microscopy. *Biophys. J.* 72:2569–2580.
38. Radhakrishnan, A., and H. M. McConnell. 1999. Condensed complexes of cholesterol and phospholipids. *Biophys. J.* 77:1507–1517.
39. Keller, S. L., A. Radhakrishnan, and H. M. McConnell. 2000. Saturated phospholipids with high melting temperatures form complexes with cholesterol in monolayers. *J. Phys. Chem. B.* 104:7522–7527.
40. Hagen, J. P., and H. M. McConnell. 1997. Liquid-liquid immiscibility in lipid monolayers. *Biochim. Biophys. Acta.* 1329:7–11.
41. Okonogi, T. M., and H. M. McConnell. 2004. Contrast inversion in the epifluorescence of cholesterol-phospholipid monolayers. *Biophys. J.* 86:880–890.
42. Hu, Y., K. Meleson, and J. Israelachvili. 2006. Thermodynamic equilibrium of domains in a two-component Langmuir monolayer. *Biophys. J.* 91:444–453.
43. Hwang, J., L. K. Tamm, C. Böhm, T. S. Ramalingam, E. Betzig, and M. Edidin. 1995. Nanoscale complexity of phospholipid monolayers investigated by near-field scanning optical microscopy. *Science.* 270:610–614.
44. Yuan, C., and L. J. Johnston. 2002. Phase evolution in cholesterol/DPPC monolayers: atomic force microscopy and near field scanning optical microscopy studies. *J. Microsc.* 205:136–146.
45. Veatch, S. L., and S. L. Keller. 2003. Separation of liquid phases in giant vesicles of ternary mixtures of phospholipids and cholesterol. *Biophys. J.* 85:3074–3083.
46. Veatch, S. L., I. V. Polozov, K. Gawrisch, and S. L. Keller. 2004. Liquid domains in vesicles investigated by NMR and fluorescence microscopy. *Biophys. J.* 86:2910–2922.
47. McConnell, H. M., and A. Radhakrishnan. 2003. Condensed complexes of cholesterol and phospholipids. *Biochim. Biophys. Acta.* 1610:159–173.
48. Loglio, G., U. Tesei, and R. Cini. 1979. Spectral data of surface viscoelastic modulus acquired via digital Fourier transformation. *J. Colloid Interf. Sci.* 71:316–320.
49. Peters, G. W. M., A. N. Zdravkov, and H. E. H. Meijer. 2005. Transient interfacial tension and dilatational rheology of diffuse polymer-polymer interfaces. *J. Chem. Phys.* 122:104901.
50. von Tscharner, V., and H. M. McConnell. 1981. Physical properties of lipid monolayers on alkylated planar glass surfaces. *Biophys. J.* 36:421–427.